Effect of velocity profile skewing on blood velocity and volume flow waveforms derived from maximum Doppler spectral velocity

Jonathan P. Mynard[1], David A. Steinman[1]

[1]Biomedical Simulation Laboratory, Department of Mechanical and Industrial Engineering, University of Toronto, Canada

Running Head: Velocity profile skewing and blood flow estimation

Address for Correspondence:
David A. Steinman
Mechanical & Industrial Engineering
University of Toronto
Toronto, Ontario, Canada, M5S 3G8
Phone: +1 416 978 7781
Fax: +1 416 978 7773
E-mail: steinman@mie.utoronto.ca

Abstract

Given evidence that fully-developed axisymmetric flow may be the exception rather than the rule, even in nominally 'straight' arteries, maximum velocity (V_{max}) may lie outside of the Doppler sample volume (SV). The link between V_{max} and derived quantities such as volume flow (Q) may therefore be more complex than commonly thought. We performed idealised virtual Doppler ultrasound on data from image-based computational fluid dynamics (CFD) models of the normal human carotid artery and investigated how velocity profile skewing and choice of sample volume affected V_{max} waveforms and derived Q variables, considering common assumptions about velocity profile shape (i.e. Poiseuille or Womersley). Severe velocity profile skewing caused substantial errors in V_{max} waveforms when using a small, centered SV, although peak V_{max} was reliably detected; errors with a long SV covering the vessel diameter were orientation dependent but lower overall. Cycle-averaged Q calculated from V_{max} was within ±15%, although substantial skewing and use of a small SV caused 10-25% underestimation. Peak Q derived from Womersley's theory was generally accurate to within ±10%. V_{max} pulsatility and resistance indexes differed from Q-based values, although Q-based resistance index could be reliably predicted. Skewing introduced significant error into V_{max}-derived Q waveforms, particularly during mid-late systole. Our findings suggest that errors in the V_{max} and Q waveforms related to velocity profile skewing and use of a small SV, or orientation-dependent errors for a long SV, may limit their use in wave analysis or for constructing characteristic or patient-specific flow boundary conditions for model studies.

Keywords: Doppler ultrasound, volume flow calculation, pulsatility index, resistance index, waveform, computational fluid dynamics, peak systolic velocity

Introduction

Routinely-acquired maximum Doppler spectral velocity (V_{max}) is widely considered to be a surrogate measure of blood volume flow (Q) and its pulsatility, and hence indirectly, of vascular impedance. Although key sources of error in Doppler ultrasound (DUS) are well-established, such as intrinsic spectral broadening, non-uniform beam insonation and operator variability (Corriveau and Johnston 2004, Evans 1985, Gill 1985, Hoskins 2011, Steinman *et al.* 2001), the relationship between V_{max} waveforms and actual Q waveforms *per se* has received less attention. Specifically, a fully-developed, axisymmetric velocity profile is often assumed in the interpretation of Doppler spectral data (Evans 1985, Hoskins 2011, Pantos *et al.* 2007). However, the presence of vessel curvature is likely to cause velocity profile skewing and thus introduce error when calculating volume flow variables (e.g. peak or cycle-averaged Q) based on classical theories derived for long straight tubes (i.e. Poiseuille or Womersley theory).

Such errors have been quantified by *in vitro* studies of secondary flows in tubes with a planar bend of constant curvature, i.e. Dean flow (Balbis *et al.* 2005, Krams *et al.* 2005, Leguy *et al.* 2009, Tortoli *et al.* 2003), but the applicability of these results in real vessels, which may contain local and compound curvatures, is unclear. In a magnetic resonance imaging study, Ponzini et al (2010) found that Womersley-based estimates of peak Q were acceptable, however the velocity profiles encountered, from 10 “healthy young volunteers”, were basically axisymmetric. By contrast, in a study of 45 older adults selected randomly from a community-based cohort, Ford et al (2008) observed skewing of cycle-averaged velocity profiles at the common carotid arteries in 60% of cases, and reaching 80% during late systole. Manbachi et al (2011) later showed that the mild, compound curvatures of the nominally ‘straight’ cervical carotid artery were sufficient to prevent flow from developing to axisymmetric, or even Dean-type profiles.

While one might expect that volume flow variables estimated from V_{max} would become progressively more inaccurate as the velocity profile becomes less axisymmetric, such a relationship has not yet been established. Coupled with this issue is the possibility that the V_{max} waveform (along with derived Q variables) may be influenced by the acquisition technique employed, particularly with respect to the choice of sample volume. For example, a small sample volume is commonly placed in the center of the vessel (Brands *et al.* 1996, Irace *et al.* 2011), but for a heavily skewed velocity profile, V_{max} may lie outside this sample volume. This could have important implications for Doppler-based haemodynamic analyses that depend on the shape of the flow-velocity waveform, e.g. non-invasive wave intensity analysis (Khir *et al.* 2001, Manisty *et al.* 2009, Zambanini *et al.* 2002) or calculation of flow augmentation index (Hirata *et al.* 2006, Ochi *et al.* 2010).

In this study, we investigated the influence of velocity profile skewing and choice of sample volume on the V_{max} waveform and V_{max}-derived volume flow variables in realistic arterial geometries by performing an idealized virtual DUS on data from image-based computational models of the carotid artery.

Methods

Study Subjects and Image Acquisition

Eighteen subjects (age range, 37-84 years; mean ± SD, 58 ± 15 years) with apparently healthy carotid arteries were selected from the Baltimore Longitudinal Study of Aging (Ferrucci 2008), a cohort representing ‘normal vascular aging’ in the VALIDATE study (Vascular Aging – The Link That Bridges Age To Atherosclerosis). The study was approved by institutional review boards and subjects provided written informed consent. Contrast-enhanced angiograms (CEMRA) and phase contrast (PC) MRI sequences were acquired at 3.0 Tesla field strength using surface radiofrequency (RF) coils. Scan parameters have been reported by Manbachi et al (2011) and Hoi et al (2010).

Computational Fluid Dynamics

To construct model geometry, the right carotid bifurcation was segmented semi-automatically from CEMRA images using Level Set methods as implemented in the open-source Vascular Modelling ToolKit (www.vmtk.org). The common carotid artery (CCA) was segmented to its thoracic origin. In six cases there was insufficient contrast to accurately segment a portion of the thoracic CCA owing to RF coil intensity profile. In these cases, the point at which the segmented lumen surface was subjectively rough was first identified (Px). Below this point the centreline of the segmentation, being relatively immune to the surface roughness, was used as the path along which the vessel boundary was extruded from Px down to the CCA origin.

CFD was performed with a validated in-house solver using quadratic tetrahedral meshes (Ethier *et al.* 2000, Minev and Ethier 1998). Boundary flows were obtained from the retrospectively-gated cine PC images and prescribed at the CCA and internal carotid artery (ICA) boundaries using fully-developed pulsatile (i.e. Womersley) velocity profiles, having adjusted ICA flow by the factor CCA/(ICA+ECA) at each time point to ensure flow conservation. A traction-free boundary condition was used for the external carotid artery (ECA). Vessel walls were assumed to be rigid and blood viscosity was taken to be 0.035 cm^2/s.

Velocity Profile Extraction

Two-dimensional axial velocity profiles in the CCA were extracted from CFD data at 3, 7 and 11 maximally-inscribed sphere radii proximal to the bifurcation (Hoi *et al.* 2010), corresponding to 1.2±0.2, 2.2±0.4 and 3.3±0.5 cm from the bifurcation apex respectively, in agreement with the range of 1-3 cm typically used in CCA DUS studies (Carallo *et al.* 1999, Gnasso *et al.* 1996, Gnasso *et al.* 1997, Holdsworth *et al.* 1999). To classify the degree of velocity profile skewing, the high velocity region (HVR) of each 2D profile was defined using the algorithm described by Ford et al (2008). Briefly, clusters of pixels containing velocities at least 20% above the mean were first identified. The velocity threshold was then adjusted until the largest cluster enclosed 25% of the lumen. Using an automated algorithm, the shape of the HVR was classified as Type I (axisymmetric), Type II (skewed) or Type III (crescent), as illustrated in Fig. 1.

From the total data set, the (time-varying) velocity profiles were selected based on their cycle-averaged type: six Type I, six Type II and twelve Type III. These numbers were chosen to provide a representative sample of each profile type, rather than to mirror their relative incidences in vivo, which has been reported to be 38:24:38 (Ford *et al.* 2008). If multiple profiles from the three slice locations in a given subject had the same type, only one of those slices was included in the analysis (selected randomly).

Idealized Virtual Doppler Ultrasound

To perform an idealized virtual DUS on the 2D velocity profile data, two virtual sample volumes were defined, with dimensions estimated on the basis of a previous study of actual Doppler sample volumes (Steinman *et al.* 2004). The first was a 1.5 mm square placed in the centre of the lumen, representing a small sample volume covering only part of the vessel diameter ('SmallSV', Fig. 1), similar to that in (Gnasso *et al.* 1996). The second represented an acquisition in which the gate range covered the whole vessel diameter ('LongSV'), as in (Holdsworth *et al.* 1999, Kochanowicz *et al.* 2009). Volume flow was calculated (as described below) using the maximum velocity within each sample volume and over the full range of possible orientations (180° in 10° steps) in the case of the simulated LongSV acquisition.

Volume Flow Calculations

Following the procedure commonly performed *in vivo* when calculating Q from DUS measurements, maximum instantaneous velocity ($V_{\max}$) from each sample volume was assumed to lie on the vessel centreline and the vessel was assumed to be cylindrical with an effective radius, R. If the effects of flow pulsatility are ignored, the resulting Poiseuille velocity profile is parabolic and Q can be calculated via,

$$Q_{\mathrm{P}}(t) = \pi R^2 \frac{V_{\max}(t)}{2} \tag{1}$$

where, in our case, $R = (A/\pi)^{1/2}$, with A the lumen cross-sectional area. In reality, flow pulsatility leads to a blunting of the velocity profile as compared with Poiseuille flow. For fully-developed pulsatile flow, Womersley's theory (Womersley 1957) leads to the following analytical expression,

$$Q_{\mathrm{W}}(t) = Q_{\mathrm{P}}(t) + \mathrm{Re}\left[\sum_{k=1}^{\infty} \pi R^2 V_{\max}(t) \left(\frac{J_0(\zeta_k) - 2J_1(\zeta_k)/\zeta_k}{J_0(\zeta_k) - \zeta_k} \right) e^{i\omega_k t}\right] \tag{2}$$

where $\zeta_k = i^{3/2}\alpha_k$, $\alpha_k = R\sqrt{\omega_k \nu}$ is the Womersley number, ν is kinematic viscosity (here assumed to be 0.035 cm^2/s), ω_k is angular frequency of the k-th sinusoidal harmonic and J_0 and J_1 are first order Bessel functions of the first and second kind (Cezeaux and van Grondelle 1997, Leguy *et al.* 2009). Pulsatility index (PI) and resistance index (RI) were calculated as (Gosling *et al.* 1971, Pourcelot 1976),

$$\mathrm{PI} = \frac{Q_{\mathrm{peak}} - Q_{\min}}{Q_{\mathrm{av}}} \quad , \quad \mathrm{RI} = \frac{Q_{\mathrm{peak}} - Q_{\min}}{Q_{\mathrm{peak}}} \tag{3}$$

where Q_{peak}, $Q_{\min}$ and Q_{av} are the peak, minimum and average volume flows over the cardiac cycle. Note that these indexes are here calculated using features of the Q waveform rather than the V_{max} waveform. The latter is more commonly used in clinical research, but may be confounded by velocity profile skewing. Waveform feature points were defined as in (Ford *et al.* 2005, Holdsworth *et al.* 1999). Due to the rigid wall assumption in the CFD simulations, cross-sectional area was constant and hence all results pertaining to Q in this study equally apply to the estimation of mean velocity from V_{max}.

To avoid confusion, throughout this manuscript 'maximum' refers to the greatest instantaneous value (for the velocity spectrum), while 'peak' refers to the largest value during the cardiac cycle (for the V_{max} and Q waveforms).

Results

Cycle-averaged velocity profiles obtained from CFD are shown in Fig. 2, along with contours outlining the HVR used to classify the profile type. Cycle-averaged V_{max} detected by SmallSV was 0.5±0.7%, 2.6±2.4% and 12.2±6.5% below the true cycle-averaged V_{max} for Type I, II and III profiles respectively. For LongSV, the departure from true cycle-averaged V_{max} depended on the orientation of the sample volume, but was less than 6% in all cases and for all orientations. Greater degrees of velocity profile skewing (i.e. Type I → Type III) were associated with greater differences between true V_{max} waveforms and those obtained from SmallSV or LongSV (Fig. 3). For SmallSV, the largest instantaneous differences were 3.1±4.1%, 9.4±6.6% and 26.8±13.7%, which overall occurred 24±17 ms after peak systole; for LongSV, the differences were 4.1±5.3%, 11.8±7.1% and 15.1±8.1% for the 'worst' orientation and zero when LongSV was oriented such that true V_{max} was detected. With SmallSV and some LongSV orientations, substantial qualitative differences between true and measured V_{max} waveforms were apparent, mainly in Type III cases (Fig. 3). Nevertheless, peak systolic V_{max} was detected accurately regardless of the profile type or sample volume (mean±SD differences of 3±4% and 1±2% overall for SmallSV and LongSV respectively, maximum differences 11% and 5%).

Noting that Q_{av} calculated from Poiseuille and Womersley assumptions were identical (as expected from theory), Fig. 4A compares true and estimated Q_{av} values for SmallSV and LongSV, where data points and associated vertical bars indicate the average value and the range of values respectively over the range of LongSV orientations. For Type I and Type II profiles, and both sample volumes, Q_{av} errors were within ±15% and the median error was well below 5% (Fig. 5, left panel). Q_{av} was generally underestimated for Type III profiles, while use of LongSV halved the median error compared with SmallSV (–16% vs. –8%); however, in one instance LongSV overestimated Q_{av} by 23%.

For all profile types, Q_{peak} was underestimated by ~20% if a Poiseuille profile was assumed. Use of a Womersley profile was more accurate, as expected (median errors <5%, Fig. 4B and Fig. 5, right panel). Although the total spread of errors was greater with higher degrees of velocity profile skewing (maximum absolute errors were 7%, 16% and 35% for Type I, II and III, using LongSV), in 88% of all cases the Q_{peak} error was less than 10%. In addition, the choice of sample volume had a minor influence on Q_{peak} estimation.

PI and RI calculated from the Q waveform were underestimated by ~30% and ~10% respectively when assuming Poiseuille conditions, with the exception of Type III cases where PI errors were generally <20% (Fig. 6, see the Supplemental Figure for scatter plots). Median PI and RI errors were reduced to <5% by assuming Womersley flow conditions, again with the exception that PI was then overestimated by ~20% for Type III profiles. Overall, calculated RI displayed less error than PI and the choice of sample volume had a minor influence.

Representative Q waveforms are shown in Fig. 7. Orientation of LongSV had no effect on calculated Q waveforms for Type I, a variable effect for Type II, and an appreciable effect for Type III. Variation in the Q waveform related to LongSV orientation was negligible prior to Q_{peak}, was most pronounced in the latter half of systole, and continued throughout most of diastole. Waveforms derived from SmallSV did not always lie within the waveform envelope derived from the set of LongSV orientations, and SmallSV Q was substantially less than LongSV Q in some Type III cases during the latter half of systole (e.g. Fig. 7 D&F). Taking the average values from the LongSV orientations, Fig. 8 shows normalised errors of instantaneous Q for the group data at a number of feature points throughout the cardiac cycle. The greatest errors occurred at peak systole (P1) for the Poiseuille assumption (all flow types), and during mid-systole to early diastole (P2, M2, D1) for SmallSV (Type III).

Discussion

This study investigated the influence of velocity profile skewing on measured V_{max} waveforms and derived volume flow variables in realistic arterial geometries. By analysing data from image-based CFD models, true V_{max} and Q were known *a priori* and we were able to avoid sources of uncertainty in DUS measurements such as intrinsic spectral broadening, area estimation and operator experience. Our results therefore represent a best-case scenario in terms of measuring volume flow from V_{max} (and V_{max} itself), allowing specific assessment of how velocity profile skewing and the choice of sample volume affect the derived quantities.

V_{max} waveforms

In clinical vascular laboratories, the V_{max} waveform is measured by tracing the highest frequency in the Doppler spectrum (Gaillard *et al.* 2010) and is most commonly acquired from a small sample volume placed in the centre of the vessel (SmallSV) (Blake *et al.* 2008, Cobbold 2007, Gnasso *et al.* 2001). Use of SmallSV implicitly assumes that flow is (at least approximately) axisymmetric, with V_{max} lying on the centreline. However, our results suggest that severe velocity profile skewing, which may be common even in nominally 'straight' vessels (Ford *et al.* 2008), may cause true V_{max} to lie outside of SmallSV. Although peak V_{max} does not appear to be significantly affected by this, the detected V_{max} waveform may be substantially different from the true V_{max} waveform. Given that skewing is most severe during flow deceleration (Ford *et al.* 2008), our data suggests that the greatest underestimation of V_{max} is likely to occur during mid-late systole (Fig. 3).

Misdetection of the V_{max} waveform due to inappropriate sample volume selection in the presence of velocity profile skewing may have important implications for various haemodynamic analyses. Since flow-velocity waveforms are thought to contain important information about vascular impedance and arterial waves, these are being analysed in increasing detail, for example, with wave intensity analysis (Khir *et al.* 2001, Manisty *et al.* 2009, Zambanini *et al.* 2002) or by quantifying a 'flow augmentation index' (FAI) (Hirata *et al.* 2006, Ochi *et al.* 2010). The latter quantifies the height of the secondary (flow-)velocity peak ('P2' in Fig. 8) compared with overall velocity amplitude and, given that the secondary peak occurs during mid-late systole, FAI may be particularly sensitive to skewing-related errors. Indeed, FAI calculated using SmallSV in our Type III cases differed from true FAI (i.e. as calculated using true V_{max}) by –25±24% (range, –50% to 33%). Similar issues are likely to affect wave intensity analysis and require further study.

Two other approaches exist for choosing a sample volume and may be more likely to detect true V_{max}. The first is to interactively move the small sample volume until the highest velocity is found (Fraser *et al.* 2008, Simon *et al.* 1990); this has been called the 'max-line' velocity by Leguy et al (2009). Another approach (which we called 'LongSV') is to use a sample volume that encompasses most or all of the vessel diameter (Holdsworth *et al.* 1999, Kochanowicz *et al.* 2009). In the current study, we presented data for SmallSV and LongSV only, since the latter effectively encompasses the max-line approach and also allowed study of the effect of LongSV orientation. Based on our findings, use of max-line or LongSV sample volumes may be preferable compared with SmallSV when features of the V_{max} or Q waveforms are of interest.

Volume flow

Volume flow is not routinely measured in the clinic, but is of interest in a number of research settings (Hartley *et al.* 2010, Taylor and Steinman 2010). For example, Q is needed in "patient-specific" computational modelling studies for specifying inlet/outlet boundary conditions (Xiang *et al.* 2011). More subtly, the question of whether Doppler-derived V_{max} provides equivalent information to volume flow (or mean velocity, V_{mean}) is of fundamental importance when translating new haemodynamic analyses from the animal laboratory to clinical settings. In particular, the V_{max} waveform obtained from SmallSV has been used in place of the mean velocity waveform to calculate wave intensity and to separate haemodynamic waveforms into forward and backward components to quantify wave reflection (Khir *et al.* 2001, Manisty *et al.* 2009, Zambanini *et al.* 2002). Our study suggests that velocity profile skewing, which may be more common than is often appreciated even in 'approximately straight' vessels, may limit the use of Poiseuille or Womersley assumptions when estimating volume flow or V_{mean} from V_{max}.

Severe skewing (Type III) caused underestimation of cycle-averaged V_{max} and hence Q_{av} when using SmallSV. As might be expected, there was a negligible effect with less marked skewing (Type I or II) since true V_{max} was more reliably detected. However, aside from misdetection of V_{max}, a second source of error was the fact that the CCA velocity profile was not fully developed (Ford *et al.* 2008). Even when the cycle-averaged velocity profile was classified as axisymmetric (Type I) or mildly skewed (Type II), errors of ±15% were observed. This may be partly explained based on previous findings that cases with Type I or Type II *cycle-averaged* profiles frequently display a Type III (highly skewed) profile during flow deceleration (Ford *et al.* 2008).

Consistent with this, a disproportionate contribution to the RMS error in our data (64% for the Womersley-derived Q waveforms) occurred between peak systole and the dichrotic notch (a period covering only ~33% of the cardiac cycle).

An important principle reflected in our results and those of others (Evans 1985, Leguy *et al.* 2009) is that Womersley and Poiseuille approaches are identical when considering cycle-averaged Q, because all pulsatile harmonics in Womersley's solution have a zero mean, but not when considering transient features of the Q waveform. For this reason, Q_{peak} was consistently underestimated by ~20% under the assumption of a parabolic profile, as was found in previous studies investigating idealised geometries (Leguy *et al.* 2009, Ponzini *et al.* 2006). By contrast, the Womersley approach led to near-zero median errors for Q_{peak}. Interestingly this was the case regardless of the degree of (cycle-averaged) velocity profile skewing, most likely because significant skewing generally arises *after* peak systole (Ford *et al.* 2008). Although the range of absolute errors for Q_{peak} increased progressively from Type I to Type III, the absolute error was less than 10% in 21/24 of cases (SmallSV or LongSV). By contrast, for Q_{av}, errors of 10% or less occurred in only 10/24 (SmallSV) and 15/24 (LongSV) of cases, suggesting, in accord with Leguy et al (2009), that Q_{peak} may be more reliably estimated than Q_{av} when assuming a fully-developed velocity profile.

The relationship between the V_{max} waveform and the Q waveform has received little attention in recent literature, other than the oft-stated assumption of fully-developed flow. In canine iliac arteries, Evans and MacPherson (1982) found that the shape of waveforms from an electromagnetic flow probe and DUS "were broadly similar…but differed in details which may be important in some instances". Using an idealised representation of the brachial artery, Leguy et al (2009) reported that Womersley-derived Q waveforms were quite accurate, notwithstanding some underestimation of Q after peak systole, a finding qualitatively similar to ours.

Data presented in the current study that employed realistic CCA geometry suggests that, given an ideal DUS acquisition, use of Womersley's theory may in some cases lead to accurate Q waveforms (e.g. Fig. 7 B,C), whereas in other cases the derived waveform may exhibit substantial quantitative and qualitative departures from the true waveform (e.g. Fig. 7 D-F). Perhaps surprisingly, instantaneous Q derived via a parabolic profile were generally comparable with those derived from a Womersley profile, with the important exception of peak systole when Q was systematically underestimated (Fig. 8). Overall, the departure of estimated waveforms from the true waveform was greater in Type III cases and during mid-to-late systole (Fig. 8). Underestimation of true V_{max} by SmallSV caused Q to be underestimated by up to 50% during this time. Nevertheless, considerable error (up to ±25%) remained when using LongSV or a max-line sample volume (data not shown, see discussion above).

Flow Pulsatility

Aside from detailed waveform analysis, the flow waveform is often broadly characterized in terms of its overall pulsatility, that is, how oscillatory the flow is compared with its mean value. Specifically, the well-known pulsatility and resistance indexes (Gosling *et al.* 1971, Pourcelot 1976) are generally considered to be indicators of distal microvascular resistance (Naessen and Bakos 2001, Wladimiroff *et al.* 1986). Although PI and RI are actually determined by a number of factors (Adamson 1999) and should therefore be interpreted with caution (Batton *et al.* 1983, Czosnyka *et al.* 1996), these parameters nevertheless appear to have value (Hecher *et al.* 1995, Sharma *et al.* 2007).

Due to the ubiquity of DUS, reported PI and RI are almost universally calculated from the V_{max} waveform. However, an underlying assumption is that V_{max} pulsatility directly reflects Q pulsatility. Given that volume flow is the ultimate link between pressure and resistance (or impedance), failure of this assumption could potentially confound the correct interpretation of *in* *vivo* data. In Fig. 9, we compare Q-based PI and RI with values obtained from the V_{max} waveform (in this instance we have pooled all cases and used the true V_{max} waveform, not that obtained from a limited sample volume). Noting that use of rigid walls in the CFD models would cause some overestimation of systolic velocities (since the vessel does not expand as pressure rises), the crosses represent values obtained after approximately correcting mean and peak velocities for an assumed 10% diameter increase (Gamble *et al.* 1994); values from uncorrected velocities are shown with boxes. It can be seen that velocity-based PI underestimates the Q-based values (by 26% ± 11%) and that correction for compliance effects causes even greater underestimation (by 44% ± 26%); the underestimation of RI is less pronounced (9% ± 3%, uncorrected; 16% ± 11%, corrected). Despite this inequality of V_{max} and Q-based PI and RI, there was a linear relationship between V_{max}-derived and Q-derived indexes ($R^2 > 0.8$, $p < 0.001$ for both PI and RI), suggesting that the V_{max}-derived indexes provide a valid qualitative representation of the Q-derived indexes.

In this study, we also assessed the possibility of measuring volume flow pulsatility via the V_{max}-derived Q waveform. Estimation of RI using Womersley's theory was excellent in all cases (20/24 having errors <5%) due mainly to the accuracy of derived Q_{peak}. While PI estimates were quite accurate for Type I or II cases (all but two cases with errors <10%), most PI errors for Type III cases lay between 10% and 30%, these errors arising from the mid-late systolic skewing of the velocity profiles.

Other Doppler-based techniques for measuring volume flow

A number of other techniques for estimating Q from DUS have been described that do not depend on V_{max}. The most popular of these calculates Q as the product of vessel cross-sectional area and the mean instantaneous velocity (V_{mean}) of all scatterers passing through LongSV. Although this method has been used for Q estimation (Gill 1985, Mitchell *et al.* 2001, Sato *et al.*

2011, Scheel *et al.* 2000) and wave analysis (Niki *et al.* 2002), it is prone to substantial errors related to a number of factors, notably non-uniform sonification of the lumen due to a limited beam width (Burns 1992, Evans 1985, Evans *et al.* 1989, Hoskins 1990). Based on our findings, LongSV orientation is also likely to influence Q values derived from V_{mean} in the presence of velocity profile skewing. In addition, it should be noted that V_{max} can be measured more reliably than V_{mean} (Evans *et al.* 1989), hence our interest in using the former.

A variety of multi-gate approaches, including colour Doppler, have also been used to derive Q (Hoeks *et al.* 1981, Picot *et al.* 1995, Soustiel *et al.* 2003, Tortoli *et al.* 1996). These measure velocity in many small sample volumes spaced across the vessel lumen. Traditionally, each velocity sample is multiplied with an associated semi-annulus area (assuming an axisymmetric profile) and then summed over all semi-annuli to obtain Q (Gill 1985). In a more recent adaptation, the axisymmetry assumption was avoided by assuming velocities follow a sinusoidal pattern around each semi-annulus, with encouraging results found in slightly curved flow phantoms (Leguy *et al.* 2009). Many other methods for estimating Q from DUS have been proposed (Cobbold 2007, Hoskins 2011, Richards *et al.* 2009) and may help overcome the need for assumptions about the velocity profile. Unfortunately these methods are either in preclinical phases of development or require special equipment or processing; in the current study, we intentionally addressed only techniques based on V_{max}, which is readily measurable in any clinical or experimental setting.

Sources of error not addressed in this study

Use of computational fluid dynamics in this study allowed us to assess the influence of velocity profile assumptions and the choice of sample volume on DUS-derived V_{max} waveforms and volume flow parameters. Although not the focus of our study, a number of other important sources of error should be acknowledged. For instance, intrinsic spectral broadening can cause substantial overestimation of V_{max} (Hoskins 2011, Steinman *et al.* 2001). Thus in a study of commercial scanners it was found that even measurement of steady flow in a straight flow phantom via V_{max} produced errors of between 10% and 40% due to spectral broadening (Winkler *et al.* 1995). Although this effect can be corrected for in principle (Steinman *et al.* 2001, Winkler *et al.* 1995), the correction depends on probe characteristics as well as focal length. Inaccuracies in measuring vessel cross-sectional area due to a non-circular lumen or limited spatial resolution, along with neglect of compliance effects, also translate to errors in calculated Q (Hoskins *et al.* 2010). In addition, since the ultrasound beam is not parallel to the direction of axial flow, any in-plane velocity components related to Dean-type flows contribute to the detected velocity signal and hence can introduce errors into axial velocity measurements (Balbis *et al.* 2005, Krams *et al.* 2005). Finally, interoperator variability constitutes a large source of error in DUS studies (Corriveau and Johnston 2004, Mikkonen *et al.* 1996). Nevertheless, our study demonstrates the non-negligible errors that would occur even for an 'ideal' DUS acquisition.

Limitations

As mentioned previously, the virtual DUS performed in this study was intentionally simplistic in order to parse out the influence of velocity profile and choice of sample volume on velocity waveform and volume flow errors. We therefore did not account for the 3D power distribution of the ultrasound beam, the exact shape of the sample volume (Steinman *et al.* 2004) or the effects of beam angle relative to the axial direction. Moreover, in practice the V_{max} follower in DUS systems does not detect the absolute maximum, but uses methods that are more robust against spectral noise (Steinman *et al.* 2001); of course, noise is not an issue when analysing CFD data.

The CFD modelling ignored wall distensibility and thus may have overestimated systolic velocities. Nevertheless, our approach was internally consistent and avoided assumptions about diameter variation when estimating Q. In practice, although wall distensibility is almost universally ignored when estimating flow from DUS, a 10% error in diameter (typical for the CCA (Gamble *et al.* 1994)) will translate to a 20% error in cross-sectional area and hence Q. This is a problem in regards to estimating not only mean diameter (Hoskins 2011), but also its variation during the cardiac cycle.

Despite the simplifications, data obtained from the MRI-based CFD models compared favourably with published normal values. The mean (range) of maximal and cycle-averaged V_{max} were 95 (58-128) cm/s and 51 (28-67) cm/s respectively, compared with 96 (50-169) cm/s and 41 (15-65) cm/s reported by Schoning et al (1994). Similarly, velocity-based PI (mean 1.37, range 0.83-1.90) and RI (0.72, 0.56-0.80) compared well with reported PI (1.72, 0.91-3.33) and RI (0.72, 0.55-0.9) (Schoning *et al.* 1994). Finally, Q_{av} obtained from PC-MRI and used for CFD boundary conditions (6.4±1.0 mL/s) were very similar to values reported by Vanninen et al (1995) in normal subjects (6.5±0.9 mL/s).

Conclusions

Velocity profile skewing, likely prevalent even in mildly/locally curved arteries such as the common carotid, can break the oft-assumed close link between V_{max} and Q. On the one hand, skewing can cause underestimation of V_{max} if a small sample volume is indiscriminately placed in the centre of the vessel. On the other hand, skewing invalidates the assumption of fully-developed axisymmetric flow. Nevertheless, if Womersley's theory is used, and assuming one could achieve an 'ideal' DUS acquisition, our data suggests errors in the range ±15% may be expected for cycle-averaged Q. Estimates of peak Q may be quite reliable (most errors < 10%) because substantial velocity profile skewing tends to emerge only after peak systole. V_{max} and Q-based indexes of pulsatility are not identical but the accuracy of Q-based RI (derived from V_{max}) is excellent. V_{max} and derived volume flow waveforms may differ substantially from the true waveforms, although the differences can be minimised by ensuring that true V_{max} is detected, e.g. by using a LongSV or 'max-line' sample volume.

Acknowledgments

The authors thank Prof. Richard Cobbold and Dr. Luis Aguilar for helpful discussions about ultrasound. This work was supported by grant NA-6727 to DAS from the Heart & Stroke Foundation of Canada. The VALIDATE study is supported by Contract No. NO1-AG-3-1003 from the National Institute on Aging, NIH and, in part, by the Intramural Research Program of the National Institute on Aging, NIH. JPM acknowledges the support of an Overseas Biomedical Training Fellowship from the National Health and Medical Research Council of Australia. DAS acknowledges the support of a Heart and Stroke Foundation Career Investigator Award.

References

Adamson SL, Arterial pressure, vascular input impedance, and resistance as determinants of pulsatile blood flow in the umbilical artery. Eur. J. Obstet. Gynecol. Reprod. Biol. 1999;84:119-25.

Balbis S, Roatta S, Guiot C, Curvature affects Doppler investigation of vessels: implications for clinical practice. Ultrasound Med. Biol. 2005;31:65-77.

Batton DG, Hellmann J, Hernandez MJ, Jeffrey Maisels M, Regional Cerebral Blood Flow, Cerebral Blood Velocity, and Pulsatility Index in Newborn Dogs. Pediatr. Res. 1983;17:908-12.

Blake JR, Meagher S, Fraser KH, Easson WJ, Hoskins PR, A Method to Estimate Wall Shear Rate with a Clinical Ultrasound Scanner. Ultrasound Med. Biol. 2008;34:760-74.

Brands PJ, Hoeks APG, Rutten MCM, Reneman RS, A noninvasive method to estimate arterial impedance by means of assessment of local diameter change and the local center-line blood flow velocity using ultrasound. Ultrasound Med. Biol. 1996;22:895-905.

Burns PN, Measuring volume flow with Doppler ultrasound—an old nut. Ultrasound Obstet. Gynecol. 1992;2:238-41.

Carallo C, Irace C, Pujia A, De Franceschi MS, Crescenzo A, Motti C, Cortese C, Mattioli PL, Gnasso A, Evaluation of common carotid hemodynamic forces. Relations with wall thickening. Hypertension 1999;34:217-21.

Cezeaux J, van Grondelle A, Accuracy of the inverse womersley method for the calculation of hemodynamic variables. Ann. Biomed. Eng. 1997;25:536-46.

Cobbold RSC. Foundations of Biomedical Ultrasound. New York: Oxford University Press, 2007.

Corriveau MM, Johnston KW, Interobserver variability of carotid Doppler peak velocity measurements among technologists in an ICAVL-accredited vascular laboratory. J. Vasc. Surg. 2004;39:735-41.

Czosnyka M, Richards HK, Whitehouse HE, Pickard JD, Relationship between transcranial Doppler-determined pulsatility index and cerebrovascular resistance: an experimental study. J. Neurosurg. 1996;84:79-84.

Ethier CR, Prakash S, Steinman DA, Leask RL, Couch GG, Ojha M, Steady flow separation patterns in a 45 degree junction. J. Fluid Mech. 2000;411:1-38.

Evans DH, On the measurement of the mean velocity of blood flow over the cardiac cycle using Doppler ultrasound. Ultrasound Med. Biol. 1985;11:735-41.

Evans DH, MacPherson DS, Some aspects of the relationship between instantaneous volumetric blood flow and continuous wave Doppler ultrasound recordings--II. A comparison between mean and maximum velocity waveforms in a canine model. Ultrasound Med. Biol. 1982;8:611-5.

Evans DH, McDicken WN, Skidmore R, Woodcock JP. Doppler Ultrasound: Physics, Instrumentation and Clinical Applications. Chichester, UK: John Wiley & Sons, 1989.

Ferrucci L, The Baltimore Longitudinal Study of Aging (BLSA): A 50-Year-Long Journey and Plans for the Future. J Gerontol A Biol Sci Med Sci 2008;63:1416-19.

Ford MD, Alperin N, Lee SH, Holdsworth DW, Steinman DA, Characterization of volumetric flow rate waveforms in the normal internal carotid and vertebral arteries. Physiol. Meas. 2005;26:477-88.

Ford MD, Xie YJ, Wasserman BA, Steinman DA, Is flow in the common carotid artery fully developed? Physiol. Meas. 2008;29:1335-49.

Fraser KH, Meagher S, Blake JR, Easson WJ, Hoskins PR, Characterization of an Abdominal Aortic Velocity Waveform in Patients with Abdominal Aortic Aneurysm. Ultrasound Med. Biol. 2008;34:73-80.

Gaillard E, Kadem L, Clavel M-A, Pibarot P, Durand L-G, Optimization of Doppler Echocardiographic Velocity Measurements Using an Automatic Contour Detection Method. Ultrasound Med. Biol. 2010;36:1513-24.

Gamble G, Zorn J, Sanders G, MacMahon S, Sharpe N, Estimation of arterial stiffness, compliance, and distensibility from M-mode ultrasound measurements of the common carotid artery. Stroke 1994;25:11-16.

Gill RW, Measurement of blood flow by ultrasound: Accuracy and sources of error. Ultrasound Med. Biol. 1985;11:625-41.

Gnasso A, Carallo C, Irace C, De Franceschi MS, Mattioli PL, Motti C, Cortese C, Association between wall shear stress and flow-mediated vasodilation in healthy men. Atherosclerosis 2001;156:171-76.

Gnasso A, Carallo C, Irace C, Spagnuolo V, De Novara G, Mattioli PL, Pujia A, Association Between Intima-Media Thickness and Wall Shear Stress in Common Carotid Arteries in Healthy Male Subjects. Circulation 1996;94:3257-62.

Gnasso A, Irace C, Carallo C, De Franceschi MS, Motti C, Mattioli PL, Pujia A, In Vivo Association Between Low Wall Shear Stress and Plaque in Subjects With Asymmetrical Carotid Atherosclerosis. Stroke 1997;28:993-98.

Gosling RG, Dunbar G, King DH, Newman DL, Side CD, Woodcock JP, Fitzgerald DE, Keates JS, Macmillan D, The Quantitative Analysis of Occlusive Peripheral Arterial Disease By a Non-Intrusive Ultrasonic Technique. Angiology 1971;22:52-55.

Hartley CJ, Reddy AK, Madala S, Entman ML, Taffet GE, Feasibility of Dual Doppler Velocity Measurements to Estimate Volume Pulsations of an Arterial Segment. Ultrasound Med. Biol. 2010;36:1169-75.

Hecher K, Campbell S, Doyle P, Harrington K, Nicolaides K, Assessment of Fetal Compromise by Doppler Ultrasound Investigation of the Fetal Circulation: Arterial, Intracardiac, and Venous Blood Flow Velocity Studies. Circulation 1995;91:129-38.

Hirata K, Yaginuma T, O'Rourke MF, Kawakami M, Age-Related Changes in Carotid Artery Flow and Pressure Pulses. Stroke 2006;37:2552-56.

Hoeks APG, Reneman RS, Peronneau PA, A Multigate Pulsed Doppler System with Serial Data Processing. IEEE Trans. Sonics Ultrason. 1981;28:242-47.

Hoi Y, Wasserman BA, Lakatta EG, Steinman DA, Effect of Common Carotid Artery Inlet Length on Normal Carotid Bifurcation Hemodynamics. J. Biomech. Eng. 2010;132:121008.

Holdsworth DW, Norley CJ, Frayne R, Steinman DA, Rutt BK, Characterization of common carotid artery blood-flow waveforms in normal human subjects. Physiol. Meas. 1999;20:219-40.

Hoskins PR, Measurement of arterial blood flow by Doppler ultrasound. Clin. Phys. Physiol. Meas. 1990;11:1.

Hoskins PR, Estimation of blood velocity, volumetric flow and wall shear rate using Doppler ultrasound. Ultrasound 2011;19:120-29.

Hoskins PR, Soldan M, Fortune S, Inglis S, Anderson T, Plevris J, Validation of Endoscopic Ultrasound Measured Flow Rate in the Azygos Vein Using a Flow Phantom. Ultrasound Med. Biol. 2010;36:1957-64.

Irace C, Carallo C, De Franceschi M, Scicchitano F, Milano M, Tripolino C, Scavelli F, Gnasso A, Human common carotid wall shear stress as a function of age and gender: a 12-year follow-up study. Age 2011:1-10.

Khir AW, Henein MY, Koh T, Das SK, Parker KH, Gibson DG, Arterial waves in humans during peripheral vascular surgery. Clin. Sci. 2001;101:749-57.

Kochanowicz J, Turek G, Rutkowski R, Mariak Z, Szydlik P, Lyson T, Krejza J, Normal reference values of ratios of blood flow velocities in internal carotid artery to those in common carotid artery using Doppler sonography. J. Clin. Ultrasound 2009;37:208-11.

Krams R, Bambi G, Guidi F, Helderman F, van der Steen AF, Tortoli P, Effect of vessel curvature on Doppler derived velocity profiles and fluid flow. Ultrasound Med. Biol. 2005;31:663-71.

Leguy C, Bosboom E, Hoeks A, van de Vosse F, Model-based assessment of dynamic arterial blood volume flow from ultrasound measurements. Med. Biol. Eng. Comput. 2009;47:641-48.

Leguy CAD, Bosboom EMH, Hoeks APG, van de Vosse FN, Assessment of blood volume flow in slightly curved arteries from a single velocity profile. J. Biomech. 2009;42:1664-72.

Manbachi A, Hoi Y, Wasserman BA, Lakatta EG, Steinman DA, On the shape of the common carotid artery with implications for blood velocity profiles. Physiol. Meas. 2011;32:1885-97.

Manisty CH, Zambanini A, Parker KH, Davies JE, Francis DP, Mayet J, McG Thom SA, Hughes AD, Differences in the Magnitude of Wave Reflection Account for Differential Effects of Amlodipine- Versus Atenolol-Based Regimens on Central Blood Pressure. An Anglo-Scandinavian Cardiac Outcome Trial Substudy. Hypertension 2009;54:724-30.

Mikkonen RHM, Kreula JM, Virkkunen PJ, Reproducibility of Doppler Ultrasound Measurements. Acta Radiol. 1996;37:545-50.

Minev PD, Ethier RC, A characteristic/finite element algorithm for the 3-D Navier-Stokes equations using unstructured grids. Comput. Meth. Appl. Mech. Eng. 1998;178:39-50.

Mitchell GF, Tardif J-C, Arnold JMO, Marchiori G, O'Brien TX, Dunlap ME, Pfeffer MA, Pulsatile Hemodynamics in Congestive Heart Failure. Hypertension 2001;38:1433-39.

Naessen T, Bakos O, Carotid vascular resistance in long-term estrogen users. Obstet. Gynecol. 2001;97:327-32.

Niki K, Sugawara M, Chang D, Harada A, Okada T, Sakai R, Uchida K, Tanaka R, Mumford CE, A new noninvasive measurement system for wave intensity: evaluation of carotid arterial wave intensity and reproducibility. Heart Vessels 2002;17:12-21.

Ochi N, Kohara K, Tabara Y, Nagai T, Kido T, Uetani E, Ochi M, Igase M, Miki T, Association of Central Systolic Blood Pressure With Intracerebral Small Vessel Disease in Japanese. Am. J. Hypertens. 2010;23:889-94.

Pantos J, Efstathopoulos E, Katritsis DG, Vascular wall shear stress in clinical practice. Curr. Vasc. Pharm. 2007;5:113-9.

Picot PA, Fruitman M, Rankin RN, Fenster A, Rapid volume flow rate estimation using transverse colour Doppler imaging. Ultrasound Med. Biol. 1995;21:1199-209.

Ponzini R, Vergara C, Redaelli A, Veneziani A, Reliable CFD-based estimation of flow rate in haemodynamics measures. Ultrasound Med. Biol. 2006;32:1545-55.

Ponzini R, Vergara C, Rizzo G, Veneziani A, Roghi A, Vanzulli A, Parodi O, Redaelli A, Womersley number-based estimates of blood flow rate in Doppler analysis: in vivo validation by means of phase-contrast MRI. IEEE Trans. Biomed. Eng. 2010;57:1807-15.

Pourcelot L. Diagnostic ultrasound for cerebral vascular diseases, In: Donald I and Levi S, eds. Present and future of diagnostic ultrasound. Rotterdam: Kooyker Scientific Publications, 1976.

Richards MS, Kripfgans OD, Rubin JM, Hall AL, Fowlkes JB, Mean Volume Flow Estimation in Pulsatile Flow Conditions. Ultrasound in Medicine & Biology 2009;35:1880-91.

Sato K, Ogoh S, Hirasawa A, Oue A, Sadamoto T, The distribution of blood flow in the carotid and vertebral arteries during dynamic exercise in humans. The Journal of Physiology 2011;589:2847-56.

Scheel P, Ruge C, Schöning M, Flow velocity and flow volume measurements in the extracranial carotid and vertebral arteries in healthy adults: reference data and the effects of age. Ultrasound Med. Biol. 2000;26:1261-66.

Schoning M, Walter J, Scheel P, Estimation of cerebral blood flow through color duplex sonography of the carotid and vertebral arteries in healthy adults. Stroke 1994;25:17-22.

Sharma VK, Tsivgoulis G, Lao AY, Malkoff MD, Alexandrov AV, Noninvasive Detection of Diffuse Intracranial Disease. Stroke 2007;38:3175-81.

Simon AC, Levenson J, Flaud P, Pulsatile flow and oscillating wall shear stress in the brachial artery of normotensive and hypertensive subjects. Cardiovasc. Res. 1990;24:129-36.

Soustiel JF, Glenn TC, Vespa P, Rinsky B, Hanuscin C, Martin NA, Assessment of Cerebral Blood Flow by Means of Blood-Flow-Volume Measurement in the Internal Carotid Artery. Stroke 2003;34:1876-80.

Steinman AH, Lui EYL, Johnston KW, Cobbold RSC, Sample volume shape for pulsed-flow velocity estimation using a linear array. Ultrasound Med. Biol. 2004;30:1409-18.

Steinman AH, Tavakkoli J, Myers JG, Cobbold RSC, Johnston KW, Sources of error in maximum velocity estimation using linear phased-array Doppler systems with steady flow. Ultrasound Med. Biol. 2001;27:655-64.

Taylor C, Steinman D, Image-Based Modeling of Blood Flow and Vessel Wall Dynamics: Applications, Methods and Future Directions. Ann. Biomed. Eng. 2010;38:1188-203.

Tortoli P, Guidi F, Guidi G, Atzeni C, Spectral velocity profiles for detailed ultrasound flow analysis. Ultrasonics, Ferroelectrics and Frequency Control, IEEE Transactions on 1996;43:654-59.

Tortoli P, Michelassi V, Bambi G, Guidi F, Righi D, Interaction between secondary velocities, flow pulsation and vessel morphology in the common carotid artery. Ultrasound Med. Biol. 2003;29:407-15.

Vanninen RL, Manninen HI, Partanen PL, Vainio PA, Soimakallio S, Carotid artery stenosis: clinical efficacy of MR phase-contrast flow quantification as an adjunct to MR angiography. Radiology 1995;194:459-67.

Winkler AJ, Wu J, Case T, Ricci MA, An Experimental Study of the Accuracy of Volume Flow Measurements Using Commercial Ultrasound Systems. J. Vasc. Tech. 1995;19:175-80.

Wladimiroff JW, Tonge HM, Stewart PA, Doppler ultrasound assessment of cerebral blood flow in the human fetus. Br. J. Obstet. Gynaecol. 1986;93:471-75.

Womersley JR. An elastic tube theory of pulse transmission and oscillatory flow in mammalian arteries: WADC Technical Report, 1957.

Xiang J, Natarajan SK, Tremmel M, Ma D, Mocco J, Hopkins LN, Siddiqui AH, Levy EI, Meng H, Hemodynamic–Morphologic Discriminants for Intracranial Aneurysm Rupture. Stroke 2011;42:144-52.

Zambanini A, Khir AW, Byrd SM, Parker KH, S.A.McG. T, Hughes AD, Wave Intensity Analysis: a Novel Non-Invasive Method for Determining Arterial Wave Transmission. Computers in Cardiology 2002;29:717-20.

Figure Legends

Fig. 1. Illustration of the idealised sample volumes (SmallSV, LongSV) in the virtual Doppler ultrasound, shown in the vessel cross-section and in relation to the three flow types seen in the common carotid artery, axisymmetric (Type I), skewed (Type II) and crescent (Type III). Velocities are represented by coloured contours.

Fig. 2. Cycle-averaged velocity profiles and high velocity region (white contour) extracted from the computational fluid dynamics data and used in the analysis, grouped by the three flow types.

Fig. 3. Comparison of true V_{max} waveforms versus V_{max} waveforms detected with SmallSV and LongSV. For LongSV, the grey shading corresponds to the range of waveforms obtained over the range of possible orientations.

Fig. 4. Scatterplots of actual versus estimated (A) cycle-averaged flow, Q_{av}; and (B) peak systolic flow, Q_{peak}. Note that Poiseuille and Womersley approximations are identical for Q_{av}. Vertical bars on the data points correspond to the range of estimated values over the range of LongSV orientations.

Fig. 5. Percentage errors in cycle-averaged flow and peak flow when calculated from the virtual Doppler ultrasound using LongSV or SmallSV, and by assuming Poiseuille or Womersley flow conditions. Red bars indicate median errors.

Fig. 6. Percentage errors in pulsatility and resistance indexes when calculated from the virtual Doppler ultrasound using LongSV or SmallSV, and by assuming Poiseuille or Womersley flow conditions. Red bars indicate median errors.

Fig. 7. Representative volume flow waveforms from the data set. A single waveform for SmallSV is shown whereas the shaded waveform envelope represents the range of waveforms obtained from LongSV for all orientations.

Fig. 8. Normalised errors in instantaneous volume flow for SmallSV and LongSV, and for Poiseuille and Womersley assumptions, represented as box plots with zero error centred on a representative normalised waveform. The thick portion of each box plot represents interquartile range and the whisker extends to the maximum and minimum errors. Feature points included are the two systolic peaks (P1, P2), the end-diastolic and end-systolic troughs (M0, M2) and four points during diastole (D1-D4), defined as in (Ford *et al.* 2005).

Fig. 9. Comparison of velocity- and flow-based pulsatility index (PI) and resistance index (RI). Squares represent values taken from the rigid-wall CFD model. Crosses represent values obtained after approximately correcting mean and peak velocity for an assumed 10% diameter variation over the cardiac cycle.

Supplemental Figure. Scatterplots of actual versus estimated (A) volume flow pulsatility index, PI, and (B) resistance index, RI. Vertical bars on the data points correspond to the range of estimated values over the range of LongSV orientations.

Fig. 1. Illustration of the idealised sample volumes (SmallSV, LongSV) in the virtual Doppler ultrasound, shown in the vessel cross-section and in relation to the three flow types seen in the common carotid artery, axisymmetric (Type I), skewed (Type II) and crescent (Type III). Velocities are represented by coloured contours.

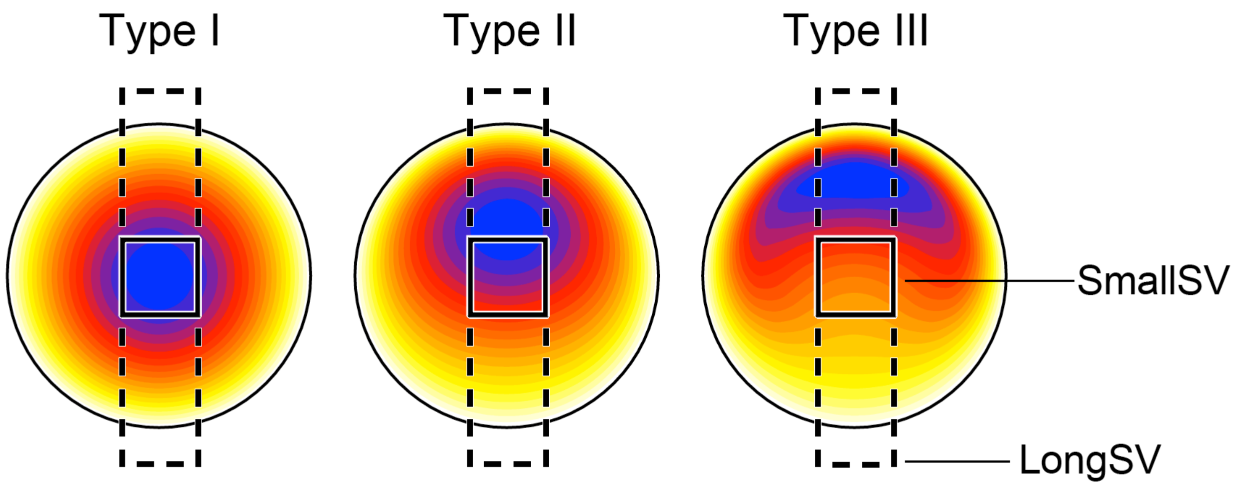

Fig. 2. Cycle-averaged velocity profiles and high velocity region (white contour) extracted from the computational fluid dynamics data and used in the analysis, grouped by the three flow types.

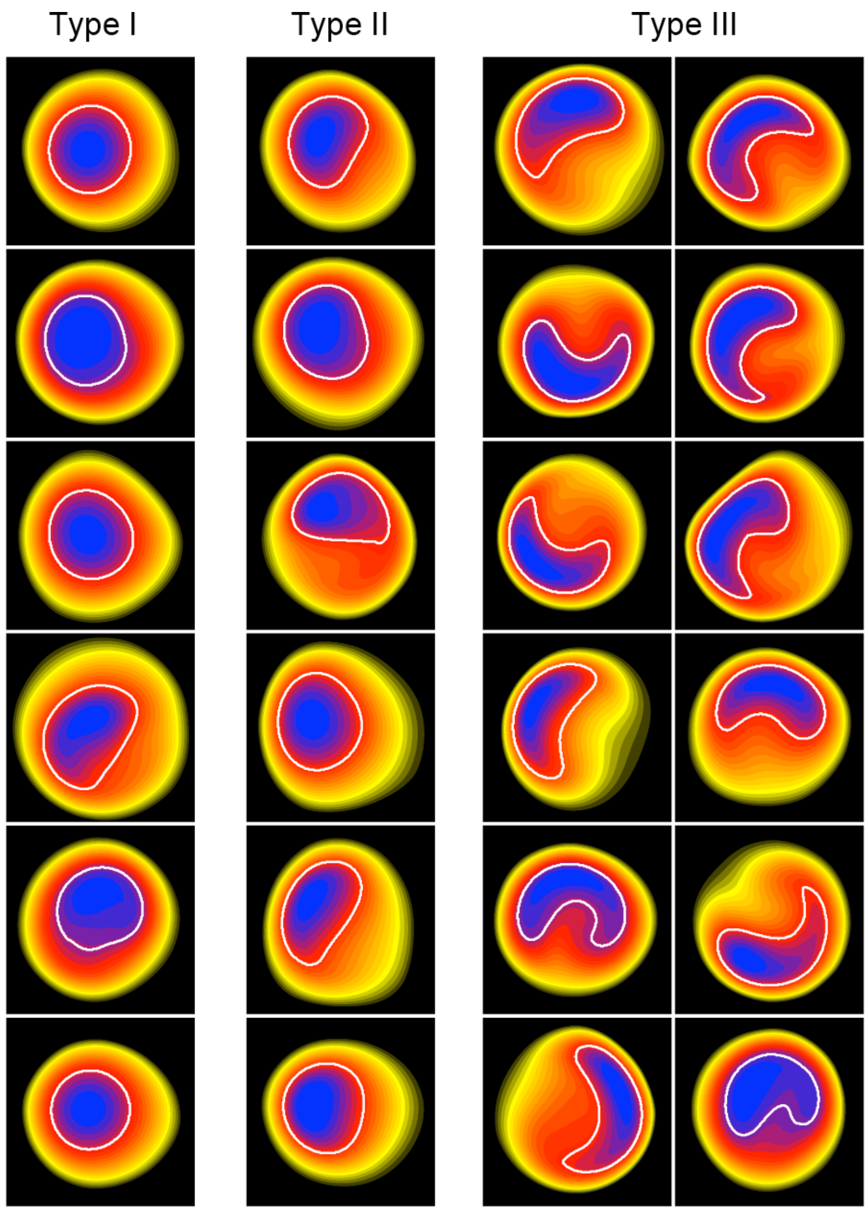

Fig. 3. Comparison of true V_{max} waveforms versus V_{max} waveforms detected with SmallSV and LongSV. For LongSV, the grey shading corresponds to the range of waveforms obtained over the range of possible orientations.

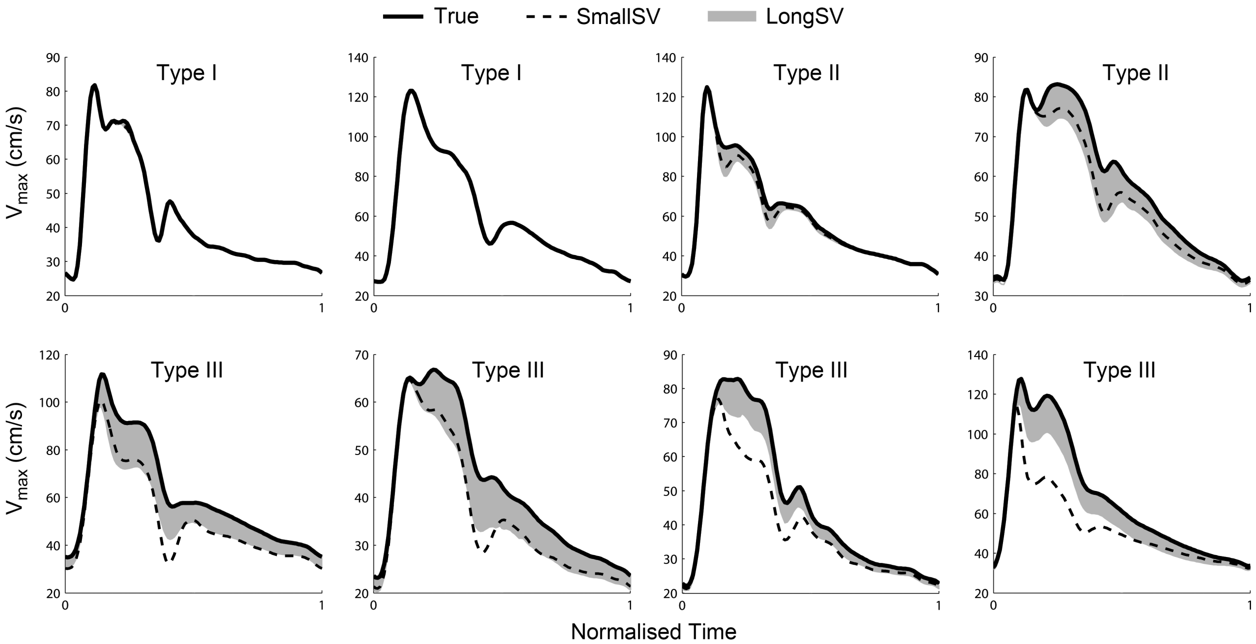

Fig. 4. Scatterplots of actual versus estimated (A) cycle-averaged flow, Q_{av}; and (B) peak systolic flow, Q_{peak}. Note that Poiseuille and Womersley approximations are identical for Q_{av}. Vertical bars on the data points correspond to the range of estimated values over the range of LongSV orientations.

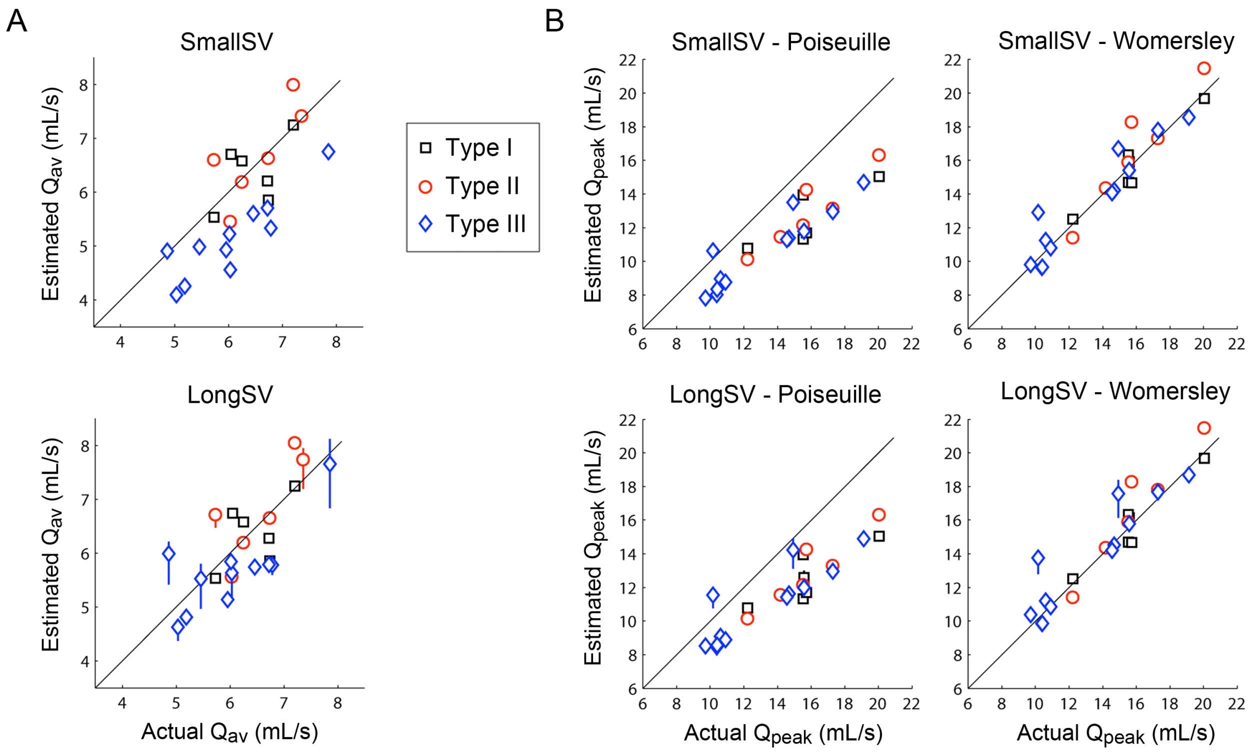

Fig. 5. Percentage errors in cycle-averaged flow and peak flow when calculated from the virtual Doppler ultrasound using LongSV or SmallSV, and by assuming Poiseuille or Womersley flow conditions. Red bars indicate median errors.

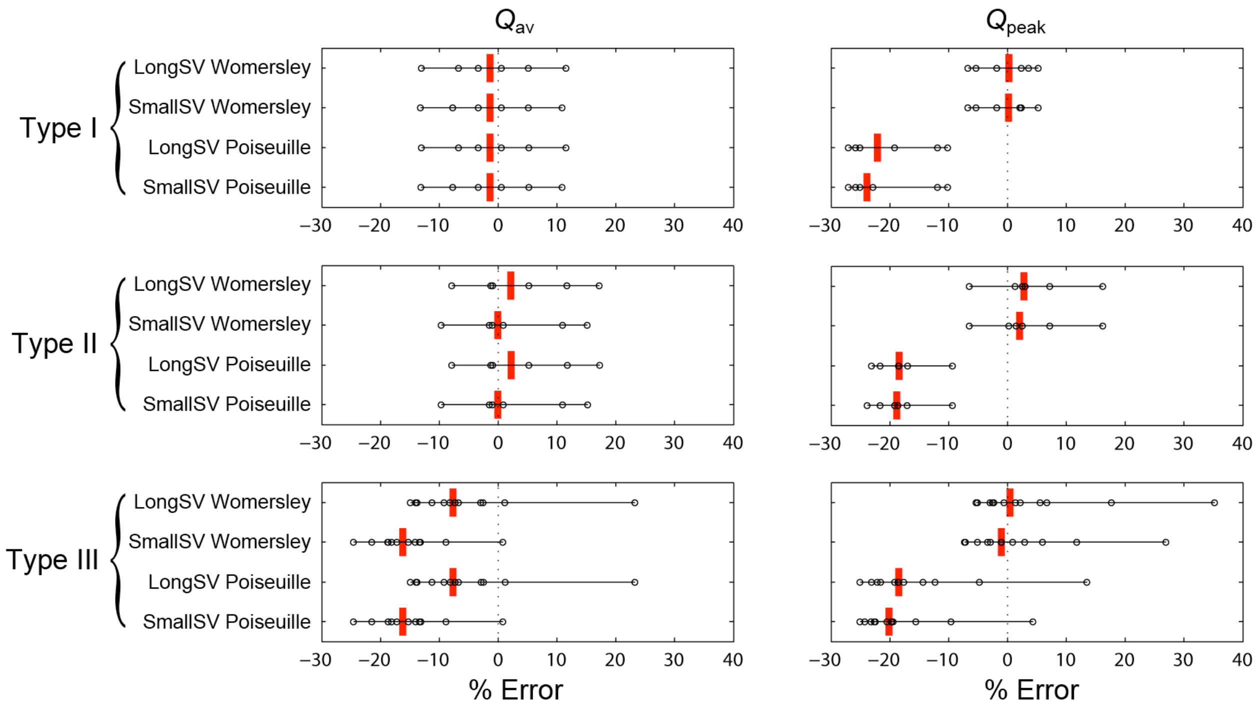

Fig. 6. Percentage errors in pulsatility and resistance indexes when calculated from the virtual Doppler ultrasound using LongSV or SmallSV, and by assuming Poiseuille or Womersley flow conditions. Red bars indicate median errors.

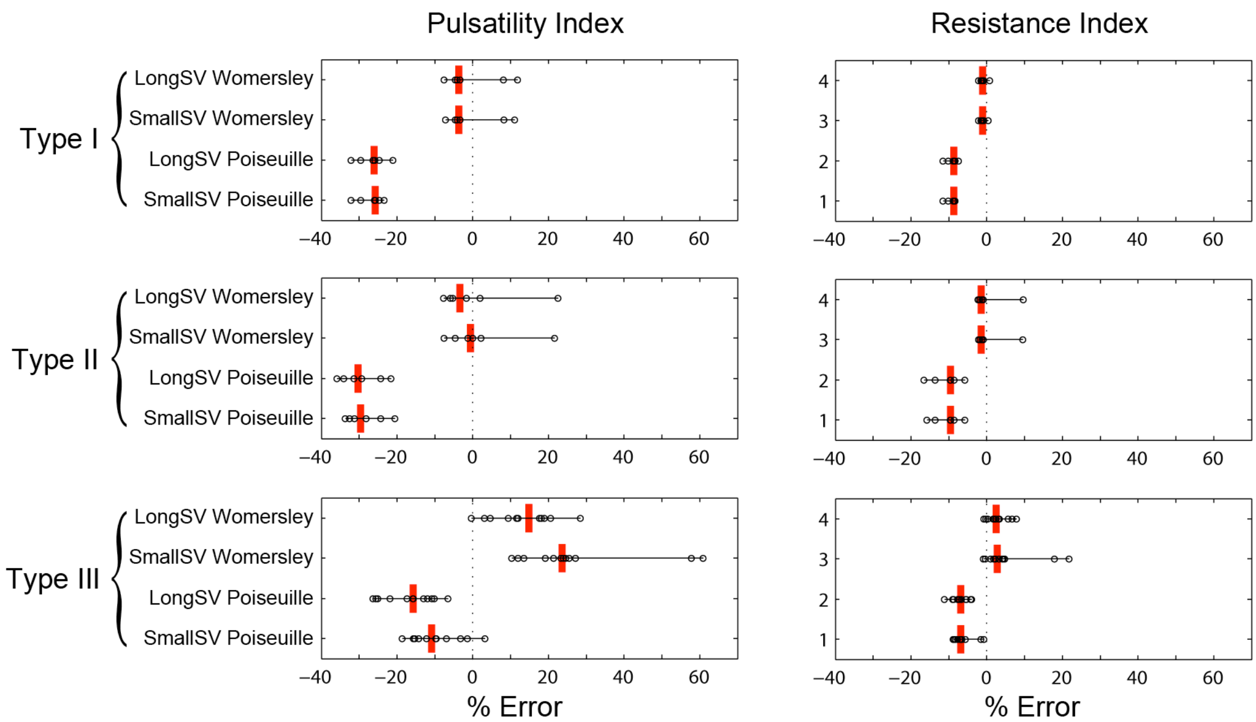

Fig. 7. Representative volume flow waveforms from the data set. A single waveform for SmallSV is shown whereas the shaded waveform envelope represents the range of waveforms obtained from LongSV for all orientations.

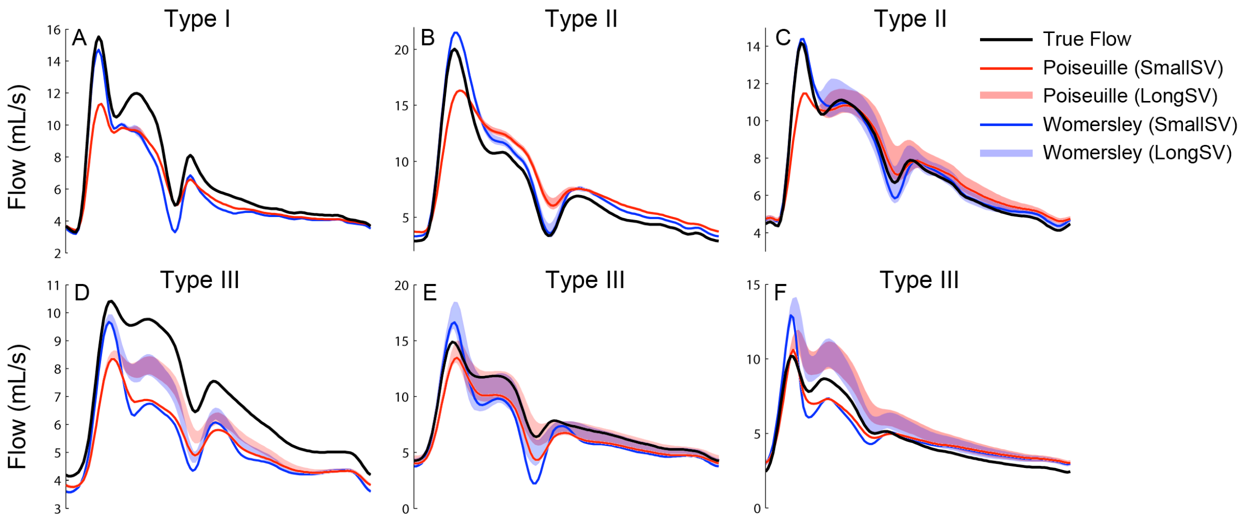

Fig. 8. Normalised errors in instantaneous volume flow for SmallSV and LongSV, and for Poiseuille and Womersley assumptions, represented as box plots with zero error centred on a representative normalised waveform. The thick portion of each box plot represents interquartile range and the whisker extends to the maximum and minimum errors. Feature points included are the two systolic peaks (P1, P2), the end-diastolic and end-systolic troughs (M0, M2) and four points during diastole (D1-D4), defined as in (Ford *et al.* 2005).

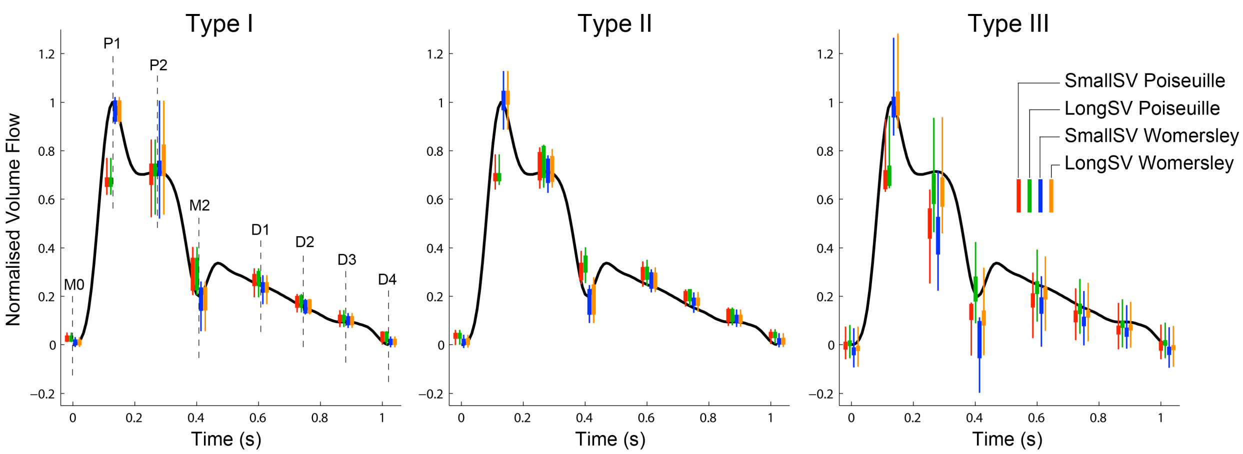

Fig. 9. Comparison of velocity- and flow-based pulsatility index (PI) and resistance index (RI). Squares represent values taken from the rigid-wall CFD model. Crosses represent values obtained after approximately correcting mean and peak velocity for an assumed 10% diameter variation over the cardiac cycle.

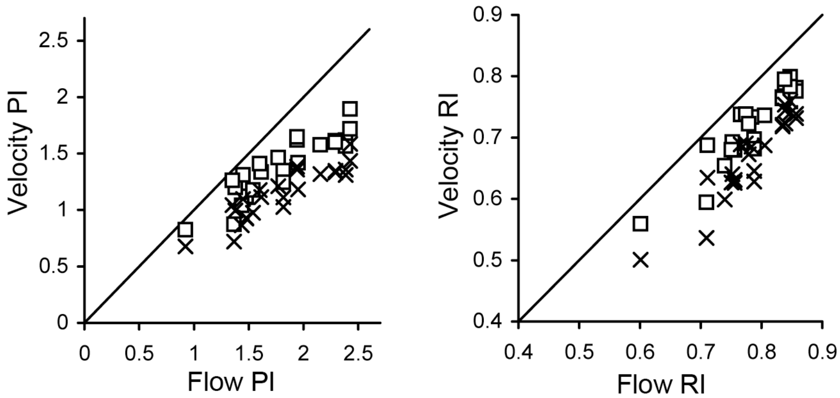

Supplemental Figure. Scatterplots of actual versus estimated (A) volume flow pulsatility index, PI, and (B) resistance index, RI. Vertical bars on the data points correspond to the range of estimated values over the range of LongSV orientations.